Mapping tissue water T_1 in the liver using the MOLLI T_1 method in the presence of fat, iron and B_0 inhomogeneity

Ferenc E Mozes MSc[1], Elizabeth M Tunnicliffe PhD[1], Ahmad Moolla MD[1,2], Thomas Marjot MD[2], Christina K Levick[1,3], Michael Pavlides MD, PhD[1,3,4], Matthew D Robson PhD[1]

[1]The University of Oxford Centre for Clinical Magnetic Resonance Research (OCMR),
University of Oxford, Level 0, John Radcliffe Hospital,
Oxford, OX3 9DU, United Kingdom
[2]Oxford Centre for Diabetes, Endocrinology and Metabolism (OCDEM),
University of Oxford, Churchill Hospital
Oxford, OX3 7LE, United Kingdom
[3]Translational Gastroenterology Unit,
University of Oxford, Level 5, John Radcliffe Hospital
Oxford, OX3 9DU, United Kingdom
[4]Oxford NIHR Biomedical Research Centre

Corresponding author:

Ferenc E Mozes
OCMR, Level 0, John Radcliffe Hospital
Oxford, OX3 9DU,
United Kingdom
Email: ferenc.mozes@cardiov.ox.ac.uk
Telephone: +44-(0)1865-234575

Grant support

The research was funded by a UK Medical Research Council Doctoral Training Award (MR/K501256/1), a Scatcherd European Scholarship, the RDM Scholars Programme, and by the National Institute for Health Research (NIHR) Oxford Biomedical Research Centre Programme. The views expressed are those of the authors and not necessarily those of the NHS, the NIHR or the Department of Health. This work is the subject of a priority UK patent application.

ABSTRACT

Modified Look-Locker Inversion recovery (MOLLI) T_1 mapping sequences can be useful in cardiac and liver tissue characterization but determining underlying water T_1 is confounded by iron, fat and frequency offsets.

This article proposes an algorithm that provides an independent water MOLLI T_1 (referred to as on-resonance water T1) that would have been measured if a subject had no fat, normal iron, and imaging had been done on resonance.

Fifteen $NiCl_2$-doped agar phantoms with different peanut oil concentrations and thirty adults with various liver disease, nineteen (63.3%) with liver steatosis, were scanned at 3 T using the shortened MOLLI (shMOLLI) T_1 mapping, multiple-echo spoiled gradient-recalled echo and ^1H MR spectroscopy sequences.

An algorithm based on Bloch equations was built in MATLAB and water shMOLLI T_1 values of both phantoms and human participants were determined. The quality of the algorithm's result was assessed by Pearson's correlation coefficient between shMOLLI T_1 values and spectroscopically determined T_1 values of the water, and by linear regression analysis.

Correlation between shMOLLI and spectroscopy-based T_1 values increased, from $r = 0.910$ ($P < 0.001$) to $r = 0.998$ ($P < 0.001$) in phantoms and from $r = 0.493$ (for iron-only correction; $P = 0.005$) to $r = 0.771$ (for iron, fat and off-resonance correction; $P < 0.001$) in patients. Linear regression analysis revealed that the determined water shMOLLI T_1 values in patients were independent of fat and iron.

It can be concluded that determination of on-resonance water (sh)MOLLI T_1 independent of fat, iron and macroscopic field inhomogeneities was possible in phantoms and human subjects.

Key words: MOLLI, shMOLLI, fat, iron, off-resonance, NAFLD

Running title: Fat correction of liver MOLLI T1

LIST OF ABBREVIATIONS

AMARES: advanced method for accurate, robust and efficient spectral fitting

bSSFP: balanced steady-state free precession

ECF: extracellular fluid volume fraction

GRAPPA: generalized autocalibrating partially parallel acquisition

GRE: gradient recalled echo

HIC: hepatic iron concentration

HLC: hepatic lipid content

HS1: hyperbolic secant 1 pulse

IR SE-EPI: inversion recovery spin echo echo-planar imaging

LISA: linearly increasing start-up angle

MCSE: multiple contrast spin echo

MOLLI: modified Look-Locker inversion recovery

NAFLD: non-alcoholic fatty liver disease

NASH: non-alcoholic steatohepatitis

shMOLLI: shortened Modified Look-Locker inversion recovery

STEAM: stimulated echo acquisition mode

PDFF: proton density fat fraction

TI: inversion time

TM: mixing time

INTRODUCTION

Quantifying the longitudinal relaxation time constant (T_1) in clinical practice is often performed using the modified Look-Locker inversion recovery (MOLLI) method [1] or its variants [2,3], due to their speed, precision, availability on clinical scanners, and good reproducibility [4]. This method has proved to be diagnostically useful both in cardiovascular MRI [5] and in liver MRI, correlating with fibrosis and inflammation [6] without the risks of biopsy [7]. Liver T_1 maps were also found to predict clinical outcomes in patients with chronic liver disease [8].

However, T_1 measured with MOLLI methods is sensitive not only to fibro-inflammatory disease but also to a number of confounding factors that change the T_1 or its measurement, either by altering the microscopic magnetic environment of the imaged tissue or by means of partial volume effects.

MOLLI and its variants generally employ a balanced steady-state free precession (bSSFP) readout [1]. The signal produced by bSSFP is dependent on the T_1 and T_2 of imaged proton species, flip angle, and off-resonance frequency [9]. The frequency dependence, in particular, can result in complex behaviour of the bSSFP signal during T_1 recovery when the imaged voxels contain both fat and water [10–12]. With typical imaging parameters and clinically relevant fat fraction, this leads to an overestimation of the liver water MOLLI T_1, at odds with the decrease expected in a simple partial volume model. This counterintuitive increase in MOLLI T_1 with fat is in addition to the effect of iron deposits that reduce T_1 and T_2 [13,14]. Magnetization transfer [15], heart rate [2], repetition time of the bSSFP readout [10] and B_0 inhomogeneity [10] also influence MOLLI T_1 values.

Removing the effect of iron on MOLLI T_1 has previously been demonstrated [16], but to best characterize fibro-inflammatory disease, off-resonance effects need to be removed, both B_0-related and chemical shift-related, to produce an on-resonance water MOLLI T_1. A disease where this might prove to be important is non-alcoholic fatty liver disease (NAFLD), a condition characterized by hepatic lipid accumulation [17]. NAFLD has a worldwide prevalence of 20-30% [18,19] and encompasses a range of pathology from non-alcoholic steatosis (simple fat accumulation) to non-alcoholic steatohepatitis (NASH; fat accumulation associated with liver inflammation), to cirrhosis. In some cases, hepatocellular carcinoma may develop [20,21]. Since both the presence of fat and fibro-inflammation causes MOLLI T_1 values to increase at 3 T

when using TR ≈ 2.3 ms, differentiating these two processes may provide additional insight into the disease and its progression.

The present study evaluates whether the confounding effect of lipids and off-resonance frequency can be, in addition to the previous correction for the effect of iron, taken into account to provide a MOLLI T_1 independent of the influence of these factors. Therefore, the target is a water MOLLI T_1 value that would have been measured if a subject had no fat, normal iron, and imaging had been done on resonance.

METHODS

Phantom experiments

Construction

Fifteen agar-based phantoms were built with varying proportions of fat and water. Phantoms were stored in 30 ml plastic sample containers (King Scientific, UK) and were built in three batches, using a recipe similar to that described by Hines et al. [22]. To vary the T_1 of water in each of the batches, $NiCl_2$ (Sigma-Aldrich, St. Louis, MO, USA) solutions with concentrations of 0.45 mM, 0.73 mM, and 1.61 mM were used. Next, 2%/weight agar (Sigma-Aldrich), 0.01%/weight sodium benzoate (Sigma-Aldrich), 43 mM sodium chloride (Sigma-Aldrich), and 43 mM sodium dodecyl sulfate (Sigma-Aldrich) were added. Each of the three solutions was boiled until it became transparent and viscous. Five sample containers were prepared for each batch, having 0%, 5%, 10%, 20%, and 30% volume of peanut oil (Tesco, UK). Each container was filled to 30 ml with water-agar solution. Each sample container was further homogenized for five minutes using an ultrasonic homogenizer (Eumax UD200SH, Hong Kong). The sodium dodecyl sulfate in the solution ensured that water and fat formed a homogenous emulsion. A sixteenth sample container was filled with 100% peanut oil. Peanut oil was chosen due to its ^{1}H spectrum resembling the ^{1}H spectrum of human subcutaneous fat [23].

Imaging

Phantoms were scanned using a Siemens Tim Trio 3 T imager (Siemens Healthineers, Erlangen, Germany) equipped with a 6-channel body matrix coil (Siemens Healthineers, Erlangen, Germany) and a spine array coil (Siemens Healthineers, Erlangen, Germany) with 24 channels, of which 9 were used. A set of multiple-echo spoiled gradient recalled echo (GRE) images were collected to compute a map of the main magnetic field variation ($\gamma\Delta B_0$). Parameters of the 2D multiple-echo GRE sequence were: flip angle (FA) = 6°, TR/TE = 22.2/1.25, 2.46, 3.69, 4.92, 6.15, 7.38, 8.61, 9.84 ms, field of view (FOV) 302 × 245 mm^2, acquisition matrix 128 × 104, phase encoding direction anterior-posterior, BW = 1180 Hz/px, bipolar gradient readout scheme and slice thickness 7 mm. The map of $\gamma\Delta B_0$ field variation was determined from a T2*-IDEAL fat-water separation method with field map estimation using a graph-cut algorithm[24,25].

T_2 values of the fat-free phantoms were determined using a multiple contrast spin echo (MCSE) experiment to quantify the effect of the agar and $NiCl_2$ on transverse relaxation. The following sequence parameters were used: TR/TE = 9000/15-480 ms in steps of 15 ms, FOV 270 × 270 mm^2, matrix 128 × 110, slice thickness 8 mm. Images with different contrasts were fitted to a mono-exponential decay model. A MOLLI variant, shortened MOLLI (shMOLLI) [2] was used to acquire a T_1 map by collecting images at 7 inversion times, over 9 simulated heart beats with 3 inversions, using the 5(1)1(1)1 scheme, i.e. the first inversion pulse was followed by five readouts and a pause with a duration of one RR interval, the second inversion pulse was followed by one readout and a pause with a duration of one RR interval and the third inversion pulse was followed by one readout. ShMOLLI parameters followed a standardized protocol (Siemens WIP 561a, Erlangen, Germany): readout FA = 35°, TR/TE = 2.52/1.05 ms, FOV 290 × 343 mm^2, matrix 192 × 182, phase encoding direction anterior-posterior, BW = 898 Hz/px, slice thickness 8 mm, 28 lines before the central line, 82 total k-space lines, shortest inversion time (TI) = 110 ms, inversion time increment 80 ms, generalized autocalibrating partially parallel acquisition (GRAPPA) [26] acceleration factor 2 with 24 reference lines, partial Fourier factor 6/8 in the phase encoding direction and simulated heart rate of 60 beats/min. The approach to steady-state was accelerated using 5 linearly increasing start-up angle (LISA) pulses [27,28] and one half-angle ramp down pulse. T_1 values were obtained by applying the shMOLLI conditional fitting algorithm [2]. All images were acquired in a coronal slice.

Spectroscopy

A set of ^1H spectra with multiple repetition times (TR) and echo times (TE) were collected using the multiple-TR, multiple-TE stimulated echo acquisition mode (STEAM) single voxel magnetic resonance spectroscopy (MRS) sequence [29] to characterize the T_1 and T_2 values of six fat peaks in the pure peanut oil phantom. Relaxation times of the pure peanut oil phantom were repeated at 20°C and 37°C. The multiple-TR, multiple-TE STEAM sequence followed the approach described by Hamilton et al. [29]: no water suppression, voxel size: 14 × 14 × 24 mm^3, mixing time (TM) = 9 ms, 24 spectra collected with TR varying between 150 and 2000 ms (150, 175, 200, 225, 250, 275, 300, 325, 350, 400, 450, 500, 600, 700, 800, 900, 1000, 1250, 1500, 2000 ms) and TE fixed at 15 ms, then 8 spectra collected with a fixed TR of 1000 ms and TE changing from 20 to 110 ms (20, 25, 30, 35, 50, 70, 90, 110 ms). A version of the sequence with multiple-TR but fixed TE = 15 ms was used to quantify individual T_1 values of water and fat peaks in the mixed water and oil phantoms. Proton density fat fractions (PDFF) were also determined from ^1H spectroscopy data. The obtained spectra were fitted

using the MATLAB-adapted version of the AMARES algorithm [30,31] and the resulting amplitudes for each peak were fitted to eq. (1), where S_{0i} is a scaling factor proportional to proton density, TE is the echo time, τ is the time from the third 90° pulse of the STEAM sequence to the end of the TR interval, i.e. the time during which the longitudinal magnetization recovery occurs and *i* is an index for each spectral peak. Table *1* shows the prior knowledge used for the AMARES fitting.

$$S_i = S_{0i}\left(1 - \exp\left(-\frac{\tau}{T_{1i}}\right)\right)\exp\left(-\frac{TE}{T_{2i}}\right) \quad (1)$$

When analysing multiple-TR only experiments, the T_{2i} were fixed to be those determined in the pure peanut oil phantom and the 0% fat phantom. PDFF was defined as the ratio of the sum of observed fat proton densities and the sum of proton densities of water and observed fat peaks, as defined by eq. (2). Here S_{0f_i} denotes the proton density of the i^{th} fat peak and S_{0w} is the proton density of water. These values were determined from fitting spectroscopy data to eq. (1).

$$PDFF[\%] = \frac{\sum_i S_{0f_i}}{S_{0w} + \sum_i S_{0f_i}} \times 100 \quad (2)$$

Simulation

A Bloch equation simulation of the shMOLLI sequence was built in MATLAB (The MathWorks, Natick, MA, USA). The simulation used the same parameters of the shMOLLI protocol that were used during the imaging experiments. The measured signal was determined as the average signal over 59 phase encode lines centered at k = 29. A hyperbolic secant 1 (HS1) inversion pulse of 10.24 ms duration was used for inversion with time-bandwidth product R = 5.48, peak B_1 = 750 Hz, and β = 3.45. The evolution of magnetization over time was simulated using Brian Hargreaves' Bloch equation simulator (http://mrsrl.stanford.edu/~brian/blochsim/).

Fat was characterized using the same six spectral peaks as evaluated by MRS. The chemical shift offset relative to water, relative amplitude, T_1 and T_2 relaxation times for each simulated component were determined from the multiple-TR, multiple-TE STEAM spectra of the peanut oil phantom.

As an initial test of the phantom model, three simulations of the water signal were carried out corresponding to the three $NiCl_2$ concentrations, using the water T_2 values measured using the MCSE experiment and average STEAM water T_1 values for the given $NiCl_2$. The water and fat bSSFP signals were then combined according to the principle of partial volumes to reflect the PDFF determined by the multiple-TR, multiple-TE STEAM spectroscopy experiment for each fat-water phantom and input to the shMOLLI T_1 fitting algorithm. These simulated shMOLLI T_1 values were then compared with the measured shMOLLI T_1 as described in the statistics section.

Determining the water shMOLLI T_1

To determine the shMOLLI T_1 of the water component of the phantoms, the simulations above were repeated with water T_1 varied over the 500 – 1600 ms range in steps of 1 ms, and the water and fat signals were again combined according to the measured PDFF. The simulated signal that satisfied the maximization problem described by eq. (*3* was selected as the closest to the measured signal, where s represents simulated bSSFP signal vectors, s_{meas} is the measured bSSFP signal vector, θ is the angle between the simulated and measured signal vectors, the numerator of the fraction represents the absolute value of the dot product of the two vectors while the denominator represents the product of the lengths of the two vectors).

$$s = \underset{s\in\mathbb{C}^7}{\operatorname{argmax}} \cos\theta_{s-s_{meas}} = \underset{s\in\mathbb{C}^7}{\operatorname{argmax}} \frac{|s \cdot s_{meas}|}{\|s\| \cdot \|s_{meas}\|} \tag{3}$$

Once the maximization was complete, an additional Bloch simulation was carried out to obtain the water-only signal that would have been generated by the MOLLI sequence on resonance. This signal was then fitted to eq. (4) to determine the apparent T_1 (T_1^*). ShMOLLI T_1 was obtained using the imperfect [32] Look-Locker correction [1,32] as described by eq. (5).

$$S_{sim} = A - B\exp\left(-\frac{TI}{T_1^*}\right) \tag{4}$$

$$T_1 = T_1^*\left(\frac{B}{A} - 1\right)$$

(5)

The T_1 obtained in the last step was considered to be the water shMOLLI T_1 value. This process was repeated for each of the phantom vials.

Patient study

Patient population

A total of 30 patients (18 female, mean age: 53 ± 8.3 years) with normal livers (N=11), alcoholic (N=1) and non-alcoholic fatty liver disease (N=18) were included. Participants were recruited from a hepatology clinic. Inclusion criteria were: adults aged between 18 and 75 years old, BMI between 25 and 50 kg/m^2, 1.5 ≤ ALT < 10 ULN, blood pressure < 160/100 mmHg and primary diagnosis of NAFLD. Exclusion criteria were: diagnosis of diabetes, blood haemoglobin < 120 mg/dl, haemorrhagic disorders, anticoagulant treatment, presence of any contraindications to an MRI exam.

The study conformed to the ethical guidelines of the 1975 Declaration of Helsinki, and was approved by the institutional research departments and the National Research Ethics Service. All patients gave written informed consent.

Imaging

Patients were scanned using the same scanner and coils as described in the phantom work and using the same imaging and spectroscopic sequences. 6 or 9 channels of the spine array coil were used, depending on patient liver size.

T2* values were obtained using a T2*-IDEAL fat-water separation method with field map estimation using a graph-cut algorithm and a signal model described by Hernando et al.[25] (eq. (6)).

$$S\left(\rho_w, \rho_f, T_2^*, TE_n\right) = e^{-\frac{TE_n}{T_2^*}}\left(\rho_w + \rho_f \sum_{k=1}^{P} \alpha_k e^{2\pi i f_k TE_n}\right) e^{-2\pi i \psi TE_n} \quad (6)$$

Here, ρ_w and ρ_f stand for the relative proton densities of water and fat, ψ represents field inhomogeneities, T_2* is common for fat and water, TE_n represents the n^{th} echo time, a_k is the relative amplitude of the k^{th} fat peak, f_k is the chemical shift offset of the k^{th} fat peak and p is the total number of fat peaks (p = 6 in our model). Eq. (7) was then applied to obtain hepatic iron concentration (HIC) values in milligrams per gram dry weight of hepatic tissue [33,34].

$$HIC[mg/g\ d.w.] = \frac{\left(\frac{1}{T_2^*} + 11\right)}{2} \times 0.0254 + 0.202$$

(7)

Hepatic shMOLLI T_1 maps had TR = 2.45 ms, bSSFP TE varied between 1.02 and 1.05 ms, FOV (270-300) × (360-400) mm^2, 24 k-space lines before the central line, 66 total k-space lines, shortest inversion time was either 100 ms or 110 ms, inversion time increment 80 ms.

Additionally, a single-voxel long-TR STEAM ^1H spectroscopy sequence [35] was also run with and without water suppression. These spectra were used to quantify PDFF. Sequence parameters were: TR was cardiac gated and at least 2 s for suppressed spectra and at least 4 s for non-suppressed spectra, TE = 10 ms, and TM = 7 ms. Voxel size was 20 × 20 × 20 mm^3 for both spectroscopy experiments. Water suppressed and non-water suppressed spectra were processed using AMARES and combined with a specialized MATLAB script [35]. When fat peaks were not visible, their amplitudes were determined using the relative amplitudes reported by Hamilton et al.[36]. PDFF was determined as the ratio of the sum of areas of fat peaks and the sum of water and fat peak areas, and was T_2-corrected using eq. (*8*)(*8*).

$$PDFF[\%] = \frac{\sum_i F_i}{We^{TE\,R_2} + \sum_i F_i} \times 100 \tag{8}$$

where F_i are the fitted amplitudes of fat peaks, W is the fitted amplitude of the water peak, TE is the spectroscopic echo time and R_2 is the transverse relaxation rate of the water in the liver in s^{-1}, given by eq. (9) [33,37,38], where HIC is measured in mg/g dry weight.

$$R_2 = \frac{1}{T_2} = (6.88 + 26.06[HIC]^{0.701} - 0.438[HIC]^{1.402}) \times 1.47 \ - 2.2\ s^{-1} \tag{9}$$

All images were acquired in a single transverse slice positioned between the tenth and eleventh thoracic vertebrae, during a breath-hold. Breath-held localized spectroscopy was performed in a voxel placed in the right lobe of the liver, away from the margin of the liver and from major blood vessels and bile ducts making sure the voxel lay in the plane used for imaging. Breath-hold lengths varied between 9 and 15 seconds for imaging and were 12 seconds for the long-TR spectroscopy acquisition and 21 seconds for the multiple-TR, multiple-TE acquisition.

The MOLLI water T_1 determination algorithm

Time-varying magnetization of water and fat were simulated using Brian Hargreaves' Bloch equation simulator (http://mrsrl.stanford.edu/~brian/blochsim/). A version of the liver model

introduced by Tunnicliffe et al. [16] was used. This model comprises an intracellular and an extracellular space, with the extracellular space divided into an interstitial fluid pool and a blood pool in fast exchange. This liver model was extended with an additional fat component and volume fractions of the extracellular fluid and the intracellular compartment were adjusted to reflect the fat fraction of the liver.

Exchange effects (both water exchange between intra and extra-cellular spaces and magnetisation transfer) were previously shown to have little influence on the simulation results [16], so the simulations presented here exclude exchange effects. Methods and results showing that exchange effects have little impact on these results can be found in the Supplementary Material.

Fat was again characterized using six spectral peaks, with the chemical shift offsets relative to water and relative amplitudes given by Hamilton et al [39]. T_1 and T_2 values of different lipid spectral peaks were fixed to values measured in the peanut oil spectra collected with the multiple-TR, multiple-TE STEAM sequence, except for the 2.76, 2.1, 1.3, and 0.9 ppm peaks of the human liver fat, for which T_2 values reported by Hamilton et al. [39] were used. T_1 of the methylene fat peak at 1.3 ppm was quantified in patients with PDFF > 5% using the multiple-TR STEAM ^{1}H MRS sequence, and a value averaged over subjects was used in the simulations. Table *2* summarizes parameters used for the simulation.

Longitudinal and transverse relaxation rates of non-fatty compartments and their iron dependence were the same as described in the main simulation by Tunnicliffe et al [16] and are shown in Table *2*. The longitudinal relaxation rate of the intracellular compartment in the absence of iron, was determined such that the simulated signal for normal HIC (1.0 mg/g dry weight [16]), 0% fat, on resonance, and normal ECF (0.4) had a fitted T_1 value equal to the shMOLLI T_1 in healthy volunteers of 717 ms [6].

Extracellular fluid volume fraction (ECF) was varied between 0.25 and (0.95 – PDFF) in steps of 0.01 and was used as a proxy for liver fibrosis. To have as good an approximation of the scanner measurement as possible, the shMOLLI RF pulse sequence was simulated using the exact inversion, repetition, and echo times, as well as number of phase encoding lines, extracted from the patient shMOLLI images. Once separate bSSFP signals were simulated for the intracellular pool, extracellular pool, and hepatic fat, they were combined as a volume fraction-weighted sum, as given by eq. (10).

$$S_{sim} = \left(ECF \cdot S_e + (1 - ECF \cdot S_i)\right) \cdot (1 - PDFF) + PDFF \cdot S_f \quad (10)$$

In this equation S_{sim} represents the overall simulated shMOLLI signal, S_e is the simulated extracellular signal, S_i is the simulated intracellular signal and S_f is the simulated fat signal.

As before, the optimal simulated signal was identified via the maximization problem described by eq. (*3*. An ROI was placed in the posterior or lateral parts of the right lobe, in a way to avoid vessels and bile ducts and as close as possible to the spectroscopy voxel. The ECF corresponding to the optimal signal was used to simulate a fat- and iron-free signal on resonance and T_1 and T_2 values of the liver compartments corresponding to normal HIC. This signal was then processed using the shMOLLI conditional fitting algorithm to obtain a water shMOLLI T_1 which should be independent of iron, fat and off-resonance frequency.

In addition, in two subjects, three separate shMOLLI T_1 maps were produced for a single liver slice: an iron-corrected, on-resonance water shMOLLI T_1 (using the full processing described in the paragraph above); iron-corrected, on resonance mixed fat-water shMOLLI T_1; and iron-corrected, inhomogeneous B_0, water shMOLLI T_1. Voxel-by-voxel PDFF values were determined from the T2*-IDEAL fat-water separation method described above followed by a magnitude-based IDEAL algorithm[40]. For one of the participants the shMOLLI T_1 map and GRE data used for this experiment were collected after a linear frequency change was induced in the right-left direction by changing the value of the shim gradient in the x direction.

The mechanisms used for both phantom and patient on-resonance water MOLLI T_1 are summarized in a block diagram shown in Figure 1.

The liver model was verified against a forward simulation of patient shMOLLI T_1 measurements by simulating the extracellular, intracellular and fat bSSFP signals. The extracellular volume fraction for each patient was estimated based on the spectroscopically measured water T_1 and using the relationship between blood volume fraction and interstitial volume fraction as given in Table *2* and given T_1 of intra- and extracellular compartments. T_1 and T_2 for the simulations were determined based on Table *2* for the intracellular and extracellular compartments, given the patient's measured HIC. The fat signal was simulated using the T_1 and T_2 values in Table *3*. These simulated signals were combined as a volume-fraction weighted sum and fit using the shMOLLI algorithm to produce the expected shMOLLI T_1 given this measured spectroscopic T_1.

Statistical analysis

Correlation between simulated and measured shMOLLI T_1 values of phantoms, as well as correlation of iron-corrected shMOLLI T_1 and iron-, fat- and off-resonance-independent water shMOLLI T_1 values with spectroscopically determined water T_1 values in patients was evaluated using Pearson's correlation coefficient. Bland-Altman plots [41] were built to evaluate agreement between water T_1s derived from STEAM spectroscopy and iron-corrected shMOLLI T_1s, and between water T_1s derived from STEAM spectroscopy and iron-, fat- and off-resonance-independent water shMOLLI T_1s. A left-tailed F-test was used to evaluate the change in the variance of T_1 differences shown on the Bland-Altman plots. All statistical hypothesis testing was performed at significance level $\alpha = 0.05$.

RESULTS

Phantom experiments

Table 3 summarizes the results of measurements made using the 100% peanut oil phantom. These values were used to characterize fat in the phantom correction algorithm.

Table 4 shows PDFF, T_1, T_2, and shMOLLI T_1 of individual fat-water phantoms. Simulated and measured phantom shMOLLI T_1 values showed good agreement ($r = 0.999$, $P < 0.001$), as reflected by Figure 2 a. Figure 2 b shows the corrected on-resonance water shMOLLI T_1 in comparison with the measured shMOLLI T_1 values. Fat-dependent shMOLLI T_1 had a clear systematic dependence on PDFF and a weaker correlation ($r = 0.910$, $P < 0.001$) with spectroscopy-based T_1 than fat-independent water shMOLLI T_1 ($r = 0.998$, $P < 0.001$). On-resonance water shMOLLI T_1 had significantly ($F = 15.003$, $P = 0.0046$) lower variance than measured shMOLLI T_1 of the difference between phantom water T_1s measured by STEAM and by shMOLLI, as shown in Figure 3.

Patient studies

Of 30 patients, 19 (63.3%) had hepatic steatosis (PDFF > 5%). The patients' fat fractions ranged from 1.53% to 20.33% and T_2^* values ranged from 6.3 ms to 37.9 ms (HIC range 0.6768 mg/g dry weight – 2.357 mg/g dry weight). Figure 4 a shows the results of the forward simulation, while Figure 4 b shows the results of the fat correction in patients. While iron-corrected shMOLLI T_1 values correlated moderately ($r = 0.493$, $P = 0.005$) with spectroscopically measured water T_1s, the fat-independent water shMOLLI T_1 determination algorithm yielded a stronger correlation with STEAM T_1 values ($r = 0.771$, $P < 0.001$). Similarly, the large variability between STEAM and iron-corrected shMOLLI T_1 introduced by the effect of fat is significantly reduced by the water shMOLLI T_1 determination algorithm ($F = 0.3448$, $P = 0.0023$), as seen on Figure 5 b.

Relaxation times of individual fat peaks used for modelling the fat compartment are summarized in Table *3*.

Table 5 contains linear regression coefficients for the dependence of shMOLLI T_1 on water STEAM T_1, PDFF and R_2^* (= $1/T_2^*$) values as well as P-values associated with these coefficients, showing that on-resonance water shMOLLI T_1 values do not show statistically significant dependence on fat.

Figure 6 shows the results of applying the algorithm pixel-by-pixel over a single slice liver shMOLLI T_1 map of two patients. The liver in the right column had, on average, HIC = 1.16 mg/g dry weight, PDFF = 15.83%, and a linearly varying frequency offset in the left-right direction with frequency offsets ranging from -50 Hz to 35 Hz, which was artificially applied by manually modifying the B_0 shim. The liver in the left column had an average HIC = 2.69 mg/g dry weight and PDFF = 8.35%.

The different effects on the overall on-resonance water-only T_1 determination are shown in Figure 7 for the participant who had the x shim manually changed over the liver. Subfigures 7b, 7c and 7d show the results of the algorithm with three different models applied on the same T_1 map of the liver: full modelling of the effects of iron, fat and B0 inhomogeneity (subfigure 7b), a model of iron and fat effects (subfigure 7c) and a model containing effects from iron and B0 inhomogeneity (subfigure 7d). The maps in the second row of Figure 7 show the T1 difference between the complete model and the partial models. As was expected, a linear variation in off-resonance frequencies over a range including both positive and negative values caused both an increase and a decrease of T_1 values [10], in this case by up to 50 ms. This under-

and overestimation of T_1 values is reflected in the difference between the iron-, fat- and off-resonance-independent water shMOLLI T_1 map and the iron and fat-independent T_1 map of subfigure 7e. When removing the effects of iron and off-resonance frequencies only, the effects of fat lead to higher-than-expected shMOLLI T_1 values, as shown in subfigure 7f, in this case by up to 250 ms.

DISCUSSION

This study describes an extension of the liver model proposed by Tunnicliffe et al. [16] to include a variable sized fat compartment and a frequency offset calculated from the GRE data used for T_2* mapping, thus obtaining a model reflecting the effects of iron, fat, and off-resonance frequencies on T_1 measured by MOLLI variants. This model then allowed the identification of an on-resonance water shMOLLI T_1 value: the value that would have been measured if subjects had 0% PDFF, and normal HIC (i.e. 1 mg/g dry weight) and were imaged in a perfectly homogeneous static magnetic field. The results of the on-resonance water shMOLLI T_1 determination algorithm showed excellent correlation with spectroscopically determined water T_1 values in phantoms, and increased, statistically-significant correlation in human participants, when compared to iron-corrected shMOLLI T_1, and reduced variance of the difference between STEAM T_1 of water and water shMOLLI T_1. While we report our results for the particular case of using the shMOLLI T1 mapping method, the water T_1 determination algorithm is equally applicable to other variants of the MOLLI acquisition method, as long as the specific timing is included in the Bloch simulations..

In addition to the assumptions of Tunnicliffe et al. regarding the homogeneous distribution of iron between the liver parenchyma and extracellular fluid, we further assumed that fat droplets in hepatocytes appear in a macrovesicular form, which is mostly prevalent in non-alcoholic fatty liver disease [42], thus not affecting the tumbling rate of water molecules in hepatocytes. We have not explored possible different relaxation mechanisms in the presence of microvesicular fat.

A further assumption was that the T_1 and T_2 relaxation times of lipid protons are independent of iron. It has been shown previously that the T_2^* of both water and fat is affected by iron [43]. However, fat diffuses much more slowly than water molecules because of the high molecular weights of constituent triglycerides, therefore, their transverse T_2 relaxation will be affected less by local field inhomogeneities. The independence of longitudinal relaxation of fat on iron is guaranteed by the lack of magnetization transfer between lipid macromolecules and water [44].

In the T2*-IDEAL model we assumed equal T2* for fat and water to ensure numerical stability of the fitting. However, the T2* of these two species might not be identical due to a susceptibility difference between them[45]. Errors in fat quantification due to this simplification

appear in ref to be small enough that they would not have caused substantial changes in our proposed water-T1 determination algorithm, particularly when PDFF is lower than 21% as shown here.

Our proposed algorithm can be implemented in at least two ways. Running the algorithm "on-line", as we have done here, by simulating patient signals every time an on-resonance water shMOLLI T_1 is needed is one option. Alternatively, one can build a look-up table a priori and look up the measured T_1 values along axes of off-resonance frequency, PDFF and HIC and then project the T_1 value along the identified ECF axis to 0 Hz off-resonance frequency, 1 mg/g dry weight HIC, and 0% PDFF. In this study, we have used ^{1}H STEAM MRS to determine PDFF locally and determine the water shMOLLI T_1 over a spectroscopic voxel of interest, as well as a complex-based T_2^*-IDEAL fat-water separation method with field map estimation followed by a magnitude-based IDEAL fat-water separation method to map fat fractions over the imaging slice, allowing determination of water shMOLLI T_1 values over the whole liver slice.

Human hepatic lipid was modelled using a hybrid model comprising chemical shift, relative amplitude, T_1 and T_2 values taken from human hepatic lipid literature and – due to its similarity to subcutaneous fat [46] – peanut oil spectroscopy measurements. However, it has been shown that the hepatic fat spectrum is different from the spectrum of abdominal subcutaneous adipose tissue [47,48], therefore, errors in the correction due to the inaccurate spectral modelling might reveal themselves at higher fat fractions where small fat peaks have a larger contribution to the overall signal. Furthermore, T_1 and T_2 relaxation times of individual fat peaks of the peanut oil spectra were determined using mono-exponential fitting, although it is known that J-coupling effects disturb the pure mono-exponential behaviour of these peaks. Since J-coupling effects were not included in any of our Bloch equation simulations and approximate relaxation times of fat peaks gave satisfactory results in phantoms, we chose not to include J-coupling effects in the patient study.

Validation of the whole multi-compartment model as an extension of the model described by Tunnicliffe et al. [16] is difficult, due to the challenge of building phantoms with multiple sub-voxel water compartments, mimicking liver tissue. However, we built an array of fat–water phantoms with two compartments and proved the validity of fat modelling and the water shMOLLI T_1 determination algorithm using these phantoms.

While the T_1 value of the tissue water can be determined spectroscopically [49], there have been attempts to also produce T_1 maps of tissue that are independent of fat. Hoad et al.[50]

reported results of a liver imaging study involving participants with fibrotic livers, in which a liver T_1 determined using an IR SE-EPI sequence was shown to be independent of fat and to correlate well with fibrosis. Pagano et al. [51] proposed an IDEAL-T_1 technique that is a modified version of SASHA [52] collecting images at several echo times for each saturation time over two breath-holds. A different approach was described by Nezafat et al. [53] that uses a modified version of the slice-interleaved T_1 (STONE) sequence [54] with spectrally water-selective inversion pulses instead of adiabatic inversion pulses. A more recent method uses the Water-Only Look-Locker Inversion recovery (WOLLI) sequence [55], that produces water-only T_1 maps by using hypergeometric inversion pulses to selectively invert water. However, our proposed method of determining water (sh)MOLLI T_1 maps independent of the effects of fat also shows promise as (sh)MOLLI is widely available and water shMOLLI T_1 values can be extracted retrospectively.

One of the limitations of this study is that water shMOLLI T_1 values of only 30 patients were determined and only 19 patients had clinically significant fat fractions in their livers, i.e. $PDFF > 5\%$. The range of fat fractions in our patient population was 1.53% – 20.33%, therefore the correction method was not validated in patients with higher liver fat fractions, although it is known that the concentration of fat in the liver can reach ~45% [56,57]. We also considered only single slice coverage of the liver, along with performing ROI-based analyses instead of mapping over the acquired slice in all but two cases. The multivariable regression analysis of on resonance water T_1 values of patients shows an unexpected, though marginal, statistically significant dependence on iron, but this was due to a single participant with high iron concentration and a very low on resonance water T_1. We also note that the forward simulation of patient shMOLLI T_1 did not completely recover the measured shMOLLI T_1. However, the gradient and intercept in Figure 4a are statistically equivalent to 1 and 0 and simulation results were spread relatively uniformly around the unity line with respect to fat and iron concentration distributions. We believe that this suggests that the remaining variability in water shMOLLI T_1 values determined by our algorithm are due to variability of the population and random measurement errors in the input model parameters, rather than any systematic errors in the approach, in which case the simulation results would be either predominantly above or below the line of unity. One principal source of random error is the recently reported dependence of multiple-TR, multiple-TE STEAM T_1 values on B_1 inhomogeneities[58]. We note that any correction process will necessarily add some noise to the data. However, the mean perpendicular distance of forward-simulated shMOLLI T1 values from the regression line (d =

41 ms) is comparable to the standard deviation observed in healthy volunteers lacking pathology (σ = 49 ms), implying that any additional variability added by the correction process is not substantially greater than the usual variation within a population.

In conclusion, we have described a four-compartment model of the liver capable of characterizing the combined effect of fat, iron, and off-resonance frequency on shMOLLI T_1 values. This enables the extraction of an on-resonance water-only shMOLLI T_1, which may help to better characterize fibro-inflammatory liver disease using T_1 mapping.

REFERENCES

1. Messroghli DR, Radjenovic A, Kozerke S, Higgins DM, Sivananthan MU, Ridgway JP. Modified Look-Locker inversion recovery (MOLLI) for high-resolution T1 mapping of the heart. *Magn Reson Med*. 2004;52(1):141-146. doi:10.1002/mrm.20110
2. Piechnik SK, Ferreira VM, Dall'Armellina E, Cochlin LE, Greiser A, Neubauer S, Robson MD. Shortened Modified Look-Locker Inversion recovery (ShMOLLI) for clinical myocardial T1-mapping at 1.5 and 3 T within a 9 heartbeat breathhold. *J Cardiovasc Magn Reson*. 2010;12(1):69. doi:10.1186/1532-429X-12-69
3. Salerno M, Janardhanan R, Jiji RS, Brooks J, Adenaw N, Mehta B, Yang Y, Antkowiak P, Kramer CM, Epstein FH. Comparison of methods for determining the partition coefficient of gadolinium in the myocardium using T1 mapping. *J Magn Reson Imaging*. 2013;38(1):217-224. doi:10.1002/jmri.23875
4. Roujol S, Weingärtner S, Foppa M, Chow K, Kawaji K, Ngo LH, Kellman P, Manning WJ, Thompson RB, Nezafat R. Accuracy, precision, and reproducibility of four T1 mapping sequences: a head-to-head comparison of MOLLI, ShMOLLI, SASHA, and SAPPHIRE. *Radiology*. 2014;272(3):683-689. doi:10.1148/radiol.14140296
5. Ferreira VM, Piechnik SK, Robson MD, Neubauer S, Karamitsos TD. Myocardial tissue characterization by magnetic resonance imaging: novel applications of T1 and T2 mapping. *J Thorac Imaging*. 2014;29(3):147-154. doi:10.1097/RTI.0000000000000077
6. Banerjee R, Pavlides M, Tunnicliffe EM, Piechnik SK, Sarania N, Philips R, Collier JD, Booth JC, Schneider JE, Wang LM, Delaney DW, Fleming KA, Robson MD, Barnes E, Neubauer S. Multiparametric magnetic resonance for the non-invasive diagnosis of liver disease. *J Hepatol*. 2014;60(1):69-77. doi:10.1016/j.jhep.2013.09.002
7. Grant A, Neuberger J. Guidelines on the use of liver biopsy in clinical practice. British Society of Gastroenterology. *Gut*. 1999;45 Suppl 4(suppl 4):IV1-IV11. doi:10.1136/GUT.45.2008.IV1
8. Pavlides M, Banerjee R, Sellwood J, Kelly C, Robson MD, Booth JC, Collier J, Neubauer S, Barnes E. Multiparametric magnetic resonance imaging predicts clinical outcomes in patients with chronic liver disease. *J Hepatol*. 2016;64(2):308-315. doi:10.1016/j.jhep.2015.10.009
9. Bieri O, Scheffler K. Fundamentals of balanced steady state free precession MRI. *J*

Magn Reson Imaging. 2013;38(1):2-11. doi:10.1002/jmri.24163

10. Mozes FE, Tunnicliffe EM, Pavlides M, Robson MD. Influence of fat on liver T_1 measurements using modified Look-Locker inversion recovery (MOLLI) methods at 3T. *J Magn Reson Imaging*. 2016;44(1):105-111. doi:10.1002/jmri.25146
11. Kellman P, Bandettini WP, Mancini C, Hammer-Hansen S, Hansen MS, Arai AE. Characterization of myocardial T1-mapping bias caused by intramyocardial fat in inversion recovery and saturation recovery techniques. *J Cardiovasc Magn Reson*. 2015;17(1):33. doi:10.1186/s12968-015-0136-y
12. Thiesson S, Thompson R, Chow K. Characterization of T1 bias from lipids in MOLLI and SASHA pulse sequences. *J Cardiovasc Magn Reson*. 2015;17(Suppl 1):W10. doi:10.1186/1532-429X-17-S1-W10
13. Ghugre NR, Coates TD, Nelson MD, Wood JC. Mechanisms of tissue-iron relaxivity: nuclear magnetic resonance studies of human liver biopsy specimens. *Magn Reson Med*. 2005;54(5):1185-1193. doi:10.1002/mrm.20697
14. Feng Y, He T, Carpenter J-P, Jabbour A, Alam MH, Gatehouse PD, Greiser A, Messroghli D, Firmin DN, Pennell DJ. In vivo comparison of myocardial T1 with T2 and T2* in thalassaemia major. *J Magn Reson Imaging*. 2013;38(3):588-593. doi:10.1002/jmri.24010
15. Robson MD, Piechnik SK, Tunnicliffe EM, Neubauer S. T1 measurements in the human myocardium: The effects of magnetization transfer on the SASHA and MOLLI sequences. *Magn Reson Med*. 2013;670:664-670. doi:10.1002/mrm.24867
16. Tunnicliffe EM, Banerjee R, Pavlides M, Neubauer S, Robson MD. A model for hepatic fibrosis: the competing effects of cell loss and iron on shortened modified Look-Locker inversion recovery T_1 (shMOLLI- T_1) in the liver. *J Magn Reson Imaging*. July 2016. doi:10.1002/jmri.25392
17. Angulo P. Nonalcoholic Fatty Liver Disease. *N Engl J Med*. 2002;346:1221-1231. doi:10.1056/NEJMra011775
18. López-Velázquez JA, Silva-Vidal K V, Ponciano-Rodríguez G, Chávez-Tapia NC, Arrese M, Uribe M, Méndez-Sánchez N. The prevalence of nonalcoholic fatty liver disease in the Americas. *Ann Hepatol*. 13(2):166-178. http://www.ncbi.nlm.nih.gov/pubmed/24552858. Accessed November 4, 2016.
19. Younossi ZM, Koenig AB, Abdelatif D, Fazel Y, Henry L, Wymer M. Global epidemiology of nonalcoholic fatty liver disease—Meta-analytic assessment of prevalence, incidence, and outcomes. *J Hepatol*. 2016;64(1):73-84.

doi:10.1002/hep.28431

20. Calzadilla Bertot L, Adams LA. The Natural Course of Non-Alcoholic Fatty Liver Disease. *Int J Mol Sci*. 2016;17(5). doi:10.3390/ijms17050774
21. FARRELL GC. Non-alcoholic steatohepatitis: What is it, and why is it important in the Asia-Pacific region? *J Gastroenterol Hepatol*. 2003;18(2):124-138. doi:10.1046/j.1440-1746.2003.02989.x
22. Hines CDG, Yu H, Shimakawa A, McKenzie CA, Brittain JH, Reeder SB. T1 Independent, T2* Corrected MRI with Accurate Spectral Modeling for Quantification of Fat: Validation in a Fat-Water-SPIO Phantom. *J Magn Reson Imaging*. 2009;30(5):1215-1222. doi:10.1002/jmri.21957
23. Yu H, Shimakawa A, McKenzie CA, Brodsky E, Brittain JH, Reeder SB. Multiecho water-fat separation and simultaneous R2* estimation with multifrequency fat spectrum modeling. *Magn Reson Med*. 2008;60(5):1122-1134. doi:10.1002/mrm.21737
24. Hernando D, Kellman P, Haldar JP, Liang Z-P. Robust water/fat separation in the presence of large field inhomogeneities using a graph cut algorithm. *Magn Reson Med*. 2009;63(1):NA-NA. doi:10.1002/mrm.22177
25. Hernando D, Kühn J-P, Mensel B, Völzke H, Puls R, Hosten N, Reeder SB. R2* estimation using "in-phase" echoes in the presence of fat: The effects of complex spectrum of fat. *J Magn Reson Imaging*. 2013;37(3):717-726. doi:10.1002/jmri.23851
26. Griswold MA, Jakob PM, Heidemann RM, Nittka M, Jellus V, Wang J, Kiefer B, Haase A. Generalized autocalibrating partially parallel acquisitions (GRAPPA). *Magn Reson Med*. 2002;47(6):1202-1210. doi:10.1002/mrm.10171
27. Nishimura DG, Vasanawala SS. Analysis and Reduction of the Transient Response in SSFP Imaging. In: *Proceedings of the International Society for Magnetic Resonance in Medicine*. ; 2000:301.
28. Deshpande VS, Shea SM, Laub G, Simonetti OP, Finn JP, Li D. 3D magnetization-prepared true-FISP: a new technique for imaging coronary arteries. *Magn Reson Med*. 2001;46(3):494-502. http://www.ncbi.nlm.nih.gov/pubmed/11550241. Accessed July 6, 2015.
29. Hamilton G, Middleton MS, Hooker JC, Haufe WM, Forbang NI, Allison MA, Loomba R, Sirlin CB. In vivo breath-hold (1) H MRS simultaneous estimation of liver proton density fat fraction, and T1 and T2 of water and fat, with a multi-TR, multi-TE sequence. *J Magn Reson Imaging*. 2015;42(6):1538-1543. doi:10.1002/jmri.24946

30. Vanhamme L, van den Boogaart A, Van Huffel S. Improved Method for Accurate and Efficient Quantification of MRS Data with Use of Prior Knowledge. *J Magn Reson*. 1997;129(1):35-43. doi:http://dx.doi.org/10.1006/jmre.1997.1244
31. Purvis LAB, Clarke WT, Biasiolli L, Valkovič L, Robson MD, Rodgers CT. OXSA: An open-source magnetic resonance spectroscopy analysis toolbox in MATLAB. Motta A, ed. *PLoS One*. 2017;12(9):e0185356. doi:10.1371/journal.pone.0185356
32. Deichmann R, Haase A. Quantification of T1 values by SNAPSHOT-FLASH NMR imaging. *J Magn Reson*. 1992;96(3):608-612. doi:10.1016/0022-2364(92)90347-A
33. Wood JC, Enriquez C, Ghugre N, Tyzka JM, Carson S, Nelson MD, Coates TD. MRI R2 and R2* mapping accurately estimates hepatic iron concentration in transfusion-dependent thalassemia and sickle cell disease patients. *Blood*. 2005;106(4):1460-1465. doi:10.1182/blood-2004-10-3982
34. Storey P, Thompson AA, Carqueville CL, Wood JC, de Freitas RA, Rigsby CK. R2* imaging of transfusional iron burden at 3T and comparison with 1.5T. *J Magn Reson Imaging*. 2007;25(3):540-547. doi:10.1002/jmri.20816
35. Rial B, Robson MD, Neubauer S, Schneider JE. Rapid quantification of myocardial lipid content in humans using single breath-hold 1H MRS at 3 Tesla. *Magn Reson Med*. 2011;66(3):619-624. doi:10.1002/mrm.23011
36. Hamilton G, Yokoo T, Bydder M, Cruite I, Schroeder ME, Sirlin CB, Middleton MS. In vivo characterization of the liver fat ^{1}H MR spectrum. *NMR Biomed*. 2011;24(7):784-790. doi:10.1002/nbm.1622
37. St Pierre TG, Clark PR, Chua-anusorn W, Fleming AJ, Jeffrey GP, Olynyk JK, Pootrakul P, Robins E, Lindeman R. Noninvasive measurement and imaging of liver iron concentrations using proton magnetic resonance. *Blood*. 2005;105(2):855-861. doi:10.1182/blood-2004-01-0177
38. Ghugre NR, Storey P, Rigsby CK, Thompson AA, Carqueville CL, Coates TD, Wood JC. Multi-field behaviour of relaxivity in an iron-rich environment. In: *Proceedings of the International Society for Magnetic Resonance in Medicine*. ; 2008:644.
39. Hamilton G, Yokoo T, Bydder M, Cruite I, Schroeder ME, Sirlin CB, Middleton MS. In vivo characterization of the liver fat 1H MR spectrum. *NMR Biomed*. 2011;24(7):784-790. doi:10.1002/nbm.1622
40. Hernando D, Hines CDG, Yu H, Reeder SB. Addressing phase errors in fat-water imaging using a mixed magnitude/complex fitting method. *Magn Reson Med*. 2012;67(3):638-644. doi:10.1002/mrm.23044

41. Altman DG, Bland JM. Measurement in Medicine: The Analysis of Method Comparison Studies. *Stat*. 1983;32(3):307. doi:10.2307/2987937
42. Reddy JK, Rao MS. Lipid metabolism and liver inflammation. II. Fatty liver disease and fatty acid oxidation. *Am J Physiol Gastrointest Liver Physiol*. 2006;290(5):G852-8. doi:10.1152/ajpgi.00521.2005
43. Horng DE, Hernando D, Reeder SB. Quantification of liver fat in the presence of iron overload. *J Magn Reson Imaging*. July 2016. doi:10.1002/jmri.25382
44. Komu M, Alanen A. Magnetization transfer in fatty and low-fat livers. *Physiol Meas*. 1994;15(3):243-250. http://www.ncbi.nlm.nih.gov/pubmed/7994202. Accessed October 14, 2016.
45. Bydder M, Hamilton G, de Rochefort L, Desai A, Heba ER, Loomba R, Schwimmer JB, Szeverenyi NM, Sirlin CB. Sources of systematic error in proton density fat fraction (PDFF) quantification in the liver evaluated from magnitude images with different numbers of echoes. *NMR Biomed*. November 2017:e3843. doi:10.1002/nbm.3843
46. Yu H, Shimakawa A, McKenzie CA, Brodsky E, Brittain JH, Reeder SB. Multiecho water-fat separation and simultaneous R*2 estimation with multifrequency fat spectrum modeling. *Magn Reson Med*. 2008;60(5):1122-1134. doi:10.1002/mrm.21737
47. Hamilton G, Schlein AN, Middleton MS, Hooker CA, Wolfson T, Gamst AC, Loomba R, Sirlin CB. In vivo triglyceride composition of abdominal adipose tissue measured by ^{1}H MRS at 3T. *J Magn Reson Imaging*. August 2016. doi:10.1002/jmri.25453
48. Lundbom J, Hakkarainen A, Söderlund S, Westerbacka J, Lundbom N, Taskinen M-R. Long-TE 1H MRS suggests that liver fat is more saturated than subcutaneous and visceral fat. *NMR Biomed*. 2011;24(3):238-245. doi:10.1002/nbm.1580
49. Hamilton G, Middleton MS, Hooker JC, Haufe WM, Forbang NI, Allison MA, Loomba R, Sirlin CB. In vivo breath-hold 1H MRS simultaneous estimation of liver proton density fat fraction, and T1 and T2 of water and fat, with a multi-TR, multi-TE sequence. *J Magn Reson Imaging*. 2015;42(6):1538-1543. doi:10.1002/jmri.24946
50. Hoad CL, Palaniyappan N, Kaye P, Chernova Y, James MW, Costigan C, Austin A, Marciani L, Gowland PA, Guha IN, Francis ST, Aithal GP. A study of T<inf>1</inf> relaxation time as a measure of liver fibrosis and the influence of confounding histological factors. *NMR Biomed*. 2015;28(6):706-714. doi:10.1002/nbm.3299
51. Pagano JJ, Chow K, Yang R, Thompson RB, Reeder null, Chow null, Higgins null,

Wacker null. Fat-water separated myocardial T1 mapping with IDEAL-T1 saturation recovery gradient echo imaging. *J Cardiovasc Magn Reson*. 2014;16(Suppl 1):P65. doi:10.1186/1532-429X-16-S1-P65

52. Chow K, Flewitt JA, Green JD, Pagano JJ, Friedrich MG, Thompson RB. Saturation recovery single-shot acquisition (SASHA) for myocardial T 1 mapping. *Magn Reson Med*. 2014;71(6):2082-2095. doi:10.1002/mrm.24878
53. Nezafat M, Roujol S, Jang J, Basha T, Botnar R. Eliminating the Impact of Myocardial Lipid Content on Myocardial T1 Mapping Using a Spectrally-Selective Inversion Pulse. In: *Proc Intl Soc Mag Reson Med*. ; 2015:2638.
54. Weingartner S, Roujol S, Akcakaya M, Basha TA, Nezafat R. Free-breathing multislice native myocardial T1 mapping using the slice-interleaved T1 (STONE) sequence. *Magn Reson Med*. 2014;124:115-124. doi:10.1002/mrm.25387
55. Garrison LD, Levick C, Pavlides M, Marjot T, Mozes F, Hodson L, Neubauer S, Robson M, Rodgers CT. Water-Only Look-Locker Inversion recovery (WOLLI) T1 mapping. In: *Proc. Intl. Soc. Mag. Reson. Med. 25*. ; 2017:0435.
56. Idilman IS, Aniktar H, Idilman R, Kabacam G, Savas B, Elhan A, Celik A, Bahar K, Karcaaltincaba M. Hepatic steatosis: quantification by proton density fat fraction with MR imaging versus liver biopsy. *Radiology*. 2013;267(3):767-775. doi:10.1148/radiol.13121360
57. Tang A, Tan J, Sun M, Hamilton G, Bydder M, Wolfson T, Gamst AC, Middleton M, Brunt EM, Loomba R, Lavine JE, Schwimmer JB, Sirlin CB. Nonalcoholic fatty liver disease: MR imaging of liver proton density fat fraction to assess hepatic steatosis. *Radiology*. 2013;267(2):422-431. doi:10.1148/radiol.12120896
58. Hamilton G, Schlein AN, Loomba R, Sirlin CB. Estimating Liver Water and Fat T1 and T2, and PDFF using Flip Angle Corrected Multi-TR, Multi-TE 1H MRS. In: *Proc Intl Soc Mag Reson Med*. ; 2018:515.
59. Hamilton G, Middleton MS, Bydder M, Yokoo T, Schwimmer JB, Kono Y, Patton HM, Lavine JE, Sirlin CB. Effect of PRESS and STEAM sequences on magnetic resonance spectroscopic liver fat quantification. *J Magn Reson Imaging*. 2009;30(1):145-152. doi:10.1002/jmri.21809

FIGURE CAPTIONS

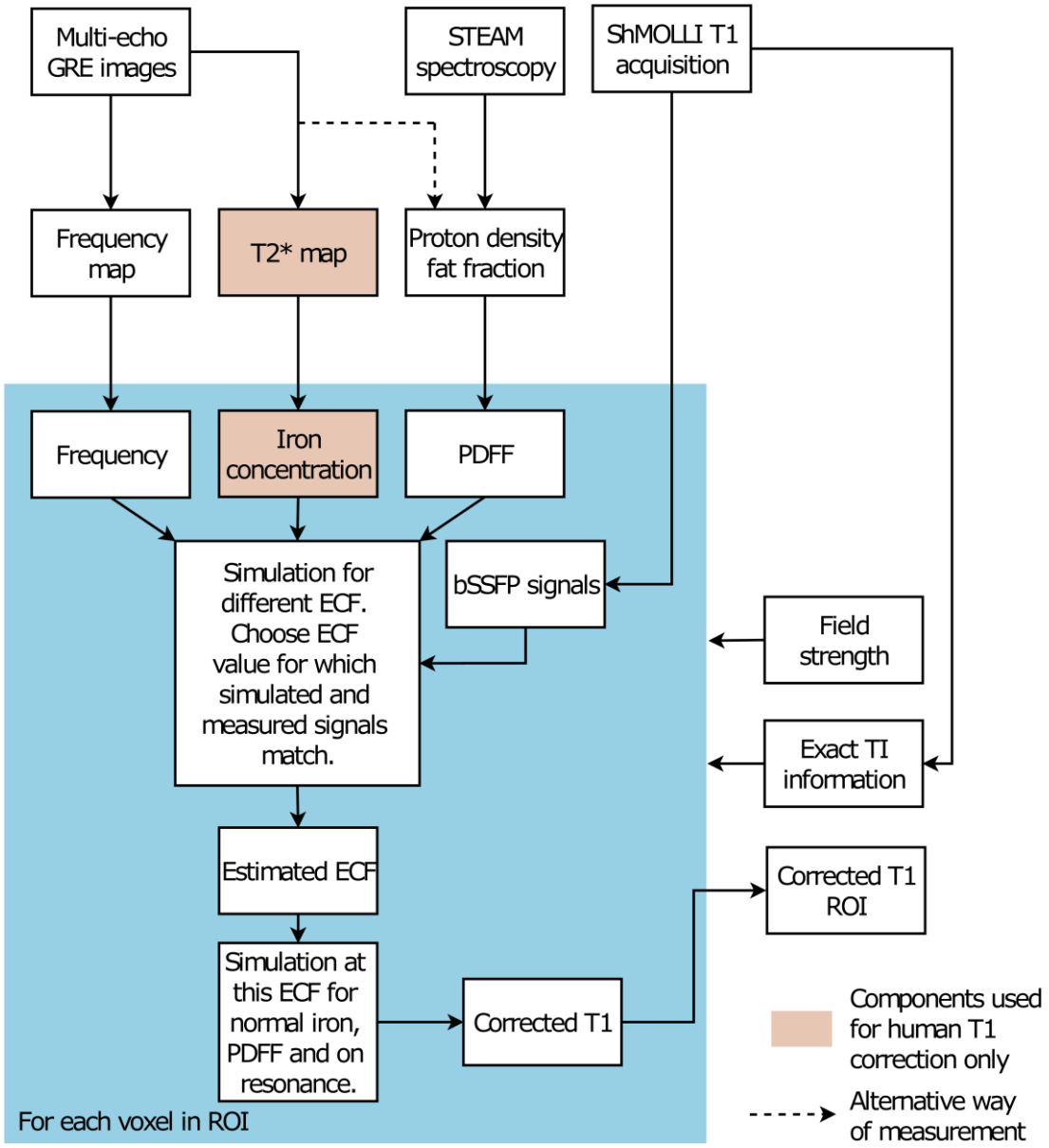

Figure 1 Block diagram of the water shMOLLI T_1 determination algorithm. In addition to the shMOLLI T_1 map, a multiple-echo GRE image set and a STEAM ^1H spectrum were also collected to derive a B_0 field map of the imaged slice and the proton density fat fraction (PDFF). When the algorithm was used to determine water shMOLLI T_1 values in patients, the GRE images were also used to generate T_2^* values and, thus, hepatic iron concentration values. Knowledge of field strength was necessary for the correct modelling of lipid peaks and the effects of iron. The actual (heart rate-dependent) inversion times were used as in the imaging experiments to eliminate possible errors caused by variable heart rates [2].

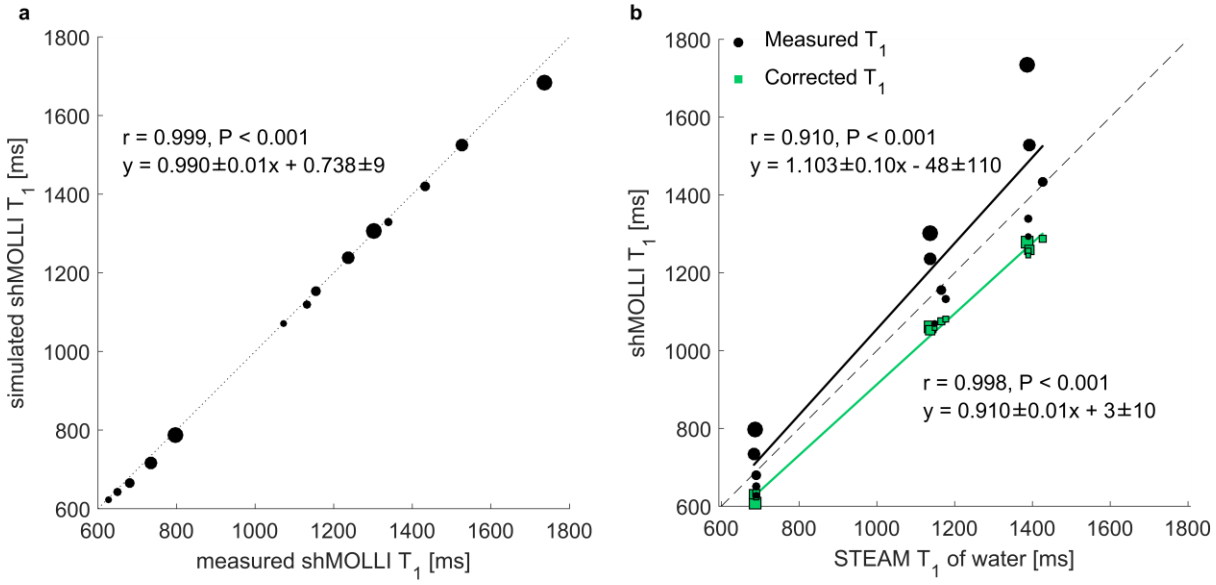

Figure 2(a) "Forward" shMOLLI simulation of the phantoms shows excellent agreement with measured shMOLLI T_1 values. (b) Correlation between shMOLLI T_1 and spectroscopy-based T_1 increases after removing the effects of fat. It is expected to obtain shMOLLI T_1s lower than T_1s obtained from spectroscopy after the determination of water shMOLLI T_1 values [32]. Points on both graphs are size-coded as a function of phantom PDFF.

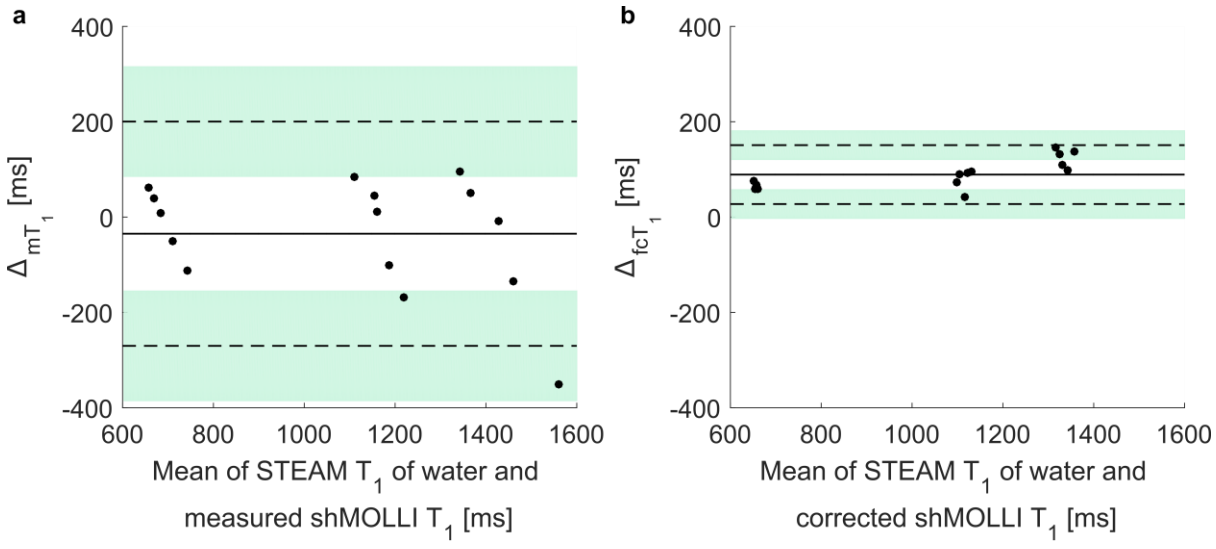

Figure 3 Bland-Altman plots showing phantom data before (a) and after (b) applying the water shMOLLI T_1 determination algorithm. The near-zero bias on subfigure a) is due to the increased shMOLLI T_1 values observed at high fat fractions, while a bias of 89 ms on subfigure b) can be explained by the expected[2] underestimation of T_1 values by the shMOLLI method. An F-test performed on the two differences shown in the subfigures revealed that the variance of the measurements was statistically significantly decreased after the removing the effects of

fat, iron and off-resonance frequency (F = 15.003, P < 0.001). Δ_{mT_1} is the difference between STEAM T_1 and the measured shMOLLI T_1; Δ_{fcT_1} is the difference between STEAM T_1 and the fat-independent water shMOLLI T_1

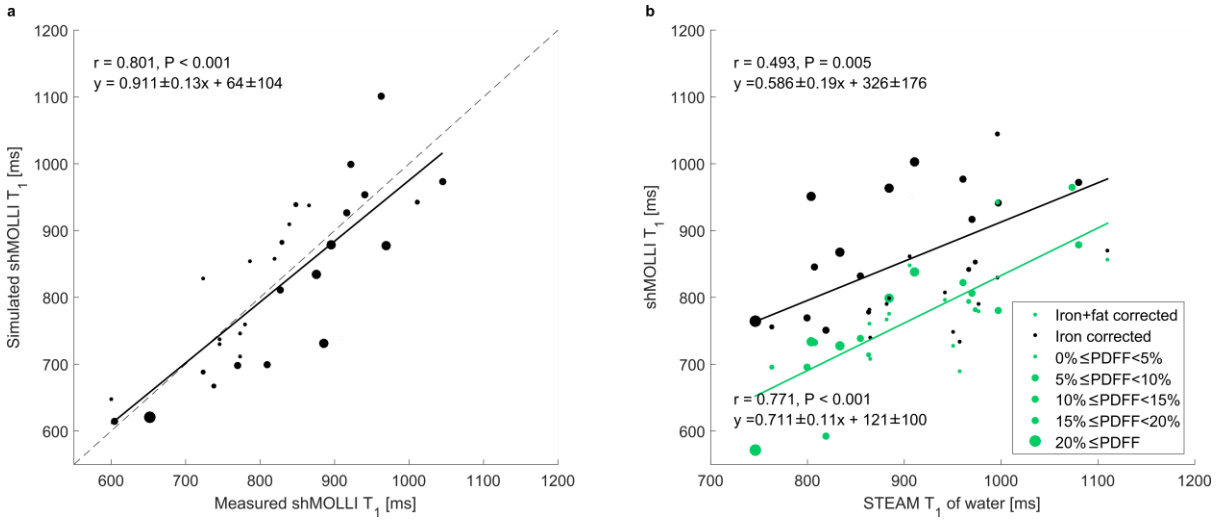

Figure 4(a) "Forward" simulation of patient shMOLLI T_1 measurements. (b) Correlation between water shMOLLI T_1 values and spectroscopically measured T_1 of the water in the liver increased after extending the initial iron-only correction to removing the effects of iron-, fat-, and off-resonance.

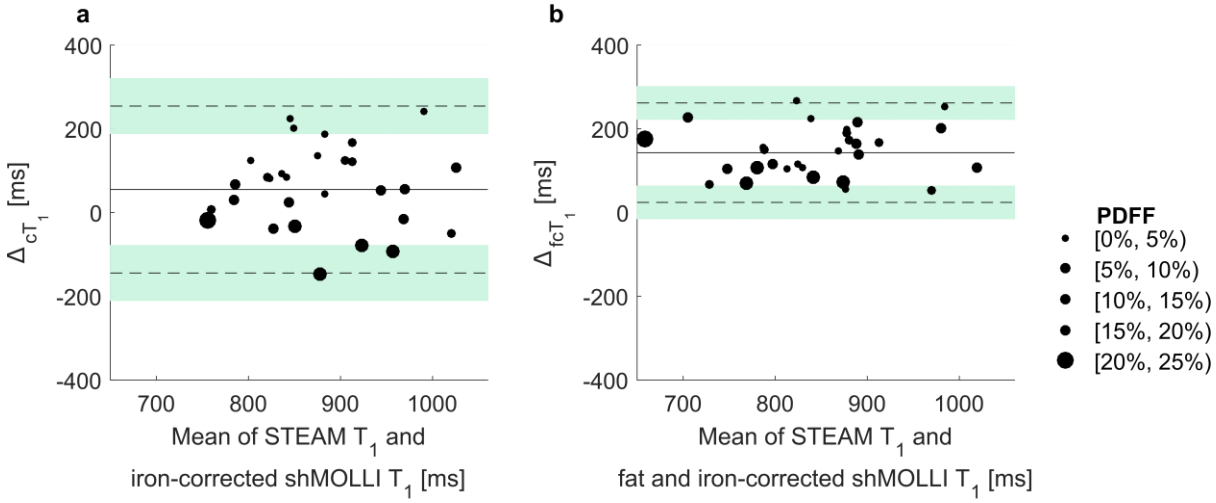

Figure 5 Bland-Altman plots of the iron-corrected (a) and iron-, fat- and off-resonance-independent patient data reveal a statistically significant (F statistic = 0.3448, p=0.0023) reduction of the variance in the difference between STEAM T_1 and shMOLLI T_1 values after removing the effects of iron, fat and B_0 inhomogeneities and remove the systematic trend for higher fat to give higher shMOLLI T_1. As in the case of phantoms, the large bias in part b is caused by the previously shown[2] underestimation of T_1s by the shMOLLI method. Δ_{cT_1} is the

difference between STEAM T_1 of the water in the liver and the iron-corrected shMOLLI T1; Δ_{fcT_1} is the difference between STEAM T_1 of the water in the liver and the iron-, fat- and off-resonance-independent water shMOLLI T_1.

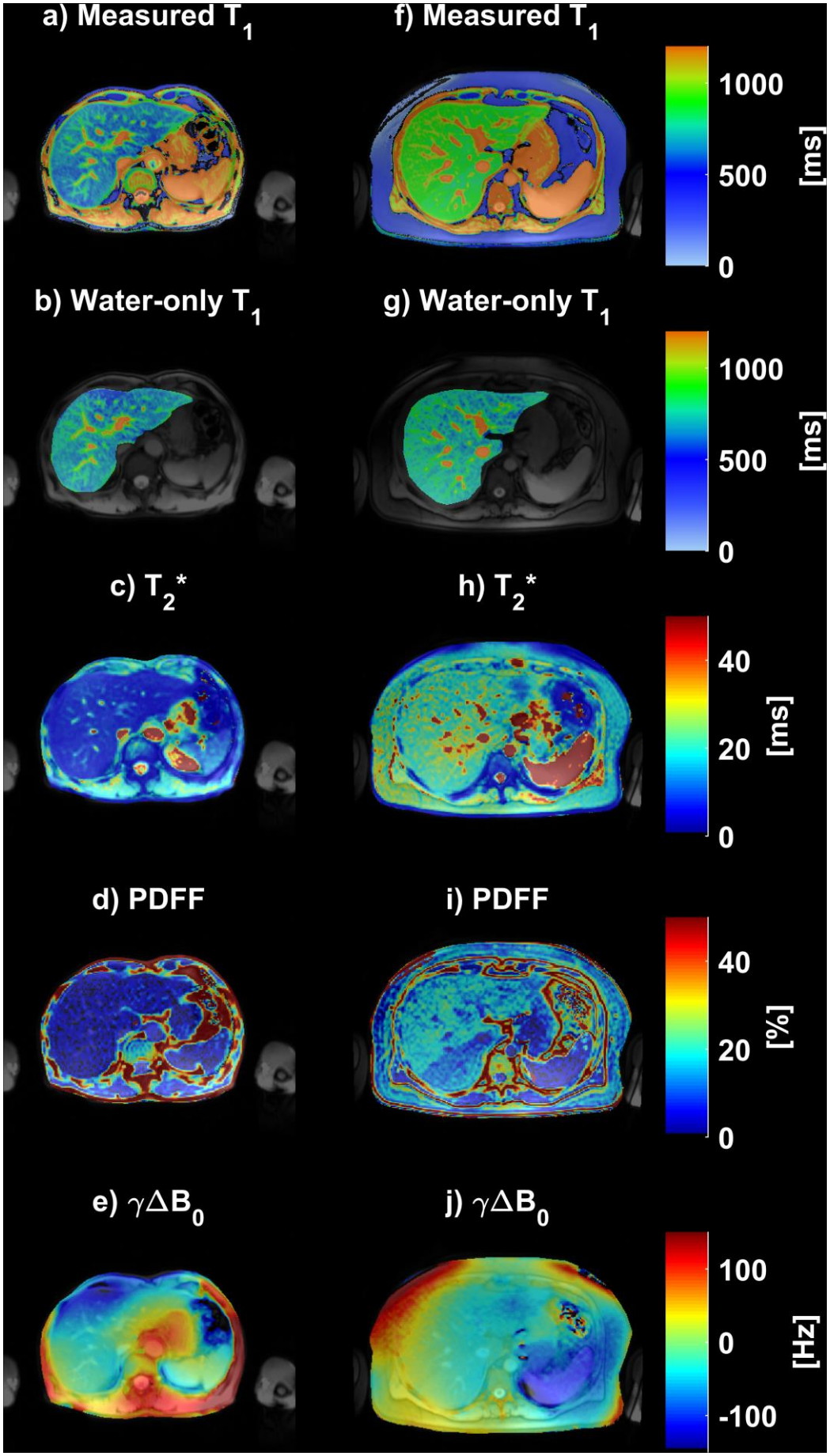
a) Measured T_1
f) Measured T_1
1000
500
0
[ms]
b) Water-only T_1
g) Water-only T_1
1000
500
0
[ms]
c) T_2*
h) T_2*
40
20
0
[ms]
d) PDFF
i) PDFF
40
20
0
[%]
e) $\gamma\Delta B_0$
j) $\gamma\Delta B_0$
100
0
-100
[Hz]

Figure 6 (a, f) Two examples of liver shMOLLI T_1 maps affected by iron, fat and B_0 inhomogeneity. (b, g) Normal liver T_1 maps resulted after removing the effects of fat, iron and B_0 inhomogeneity. The calculated T_2* maps show a homogeneous distribution of (c) increased (mean HIC = 2.69 mg/g dry weight) and (h) normal iron concentrations (mean HIC = 1.16 mg/g dry weight). Full PDFF (d – mean PDFF = 8.35 %, i – mean PDFF = 15.83 %) and B_0 field maps (e – mean $\gamma\Delta B_0$ = 1.78 Hz, j – mean $\gamma\Delta B_0$ = -8.81 Hz) are also shown.

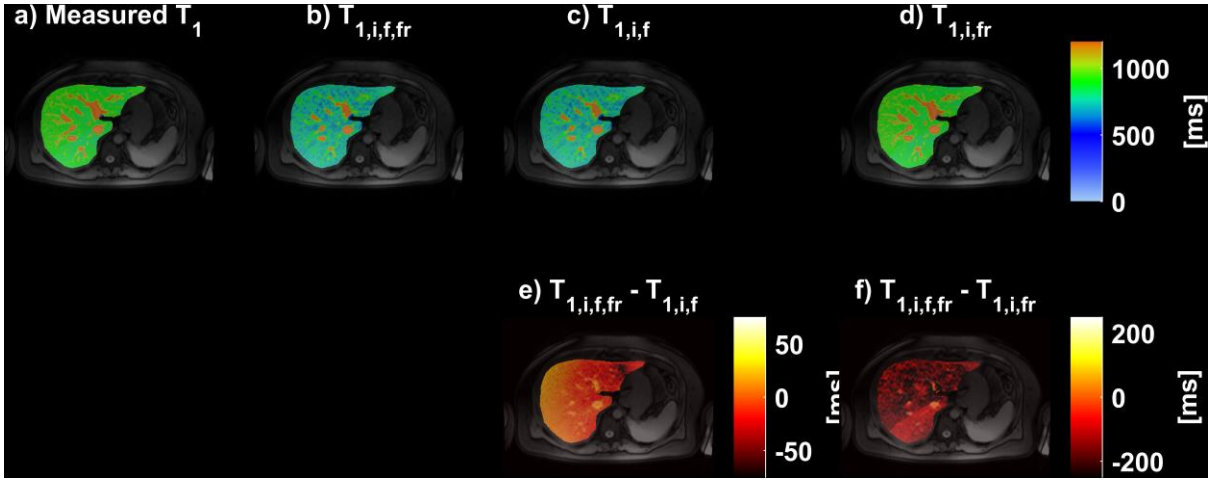

Figure 7 Three models were used in total to determine water-only shMOLLI T_1 based on a measured shMOLLI T_1 map. In addition to the full model of iron, fat and off-resonance effects (b), two additional models implemented: one without accounting for B_0 inhomogeneity and another without accounting for fat. Subfigure (c) shows the resulting T_1 map after the effects of iron and fat have been removed; subfigure

e (e) shows the difference between the T_1 map obtained by using the full model and this alternative corrected T_1 map. Removing the effects of iron and B_0 inhomogeneity only (d) yields higher-than-normal T_1 values. The difference between this alternative T_1 map and the water shMOLLI T_1 map determined using the full model (f) is explained by the effects of the fat.

TABLES

Table 1 Prior knowledge of six fat peaks used to fit peanut oil spectra

Peak number	Chemical shift [ppm]	Line shape	Line width [Hz]	Peak name
1	0.9		20	Methyl
2	1.3		40	Methylene
3	2.10	Lorentzian	40	α-carboxyl and α-olefinic
4	2.76		20	Diacyl
5	4.30		40	Glycerol
6	5.30		30	Olefinic

Table 2 Simulation parameters for the liver model at 3 Tesla.

Parameter	Value
PDFF	Proton density fat fraction as measured by ^{1}H STEAM MRS
v_C	$1 - v_E - PDFF$
v_E	Simulated from 0.25 to $(0.95 - PDFF)$
v_B	$\frac{1 - v_E - PDFF}{3}$
v_I	$v_E - v_B$
f [Hz]	As determined from the multiple-echo GRE sequence
Fat chemical shifts [ppm]	As determined by the multiple-TR, multiple-TE STEAM ^{1}H MRS sequence of peanut oil*
T_{1fat} [s]	T_1 of methylene peak determined from human ^{1}H spectra. Others as determined by the multiple-TR, multiple-TE STEAM ^{1}H MRS sequence of peanut oil*
T_{2fat} [s]	Values taken from literature [59] where available or from peanut oil spectra*
$R_{2E}\,[s^{-1}]$	$\frac{3.64v_B + 2.9v_I}{v_E} + 26.82HIC^{0.701} - 0.451HIC^{1.402}$
$R_{2C}\,[s^{-1}]$	$11.0 + 46.0HIC^{0.701} - 0.773HIC^{1.402}$
$R_{1E}\,[s^{-1}]$	$\frac{0.518v_B + 0.44v_I}{v_E} + 0.029HIC$
$R_{1C}\,[s^{-1}]$	$1.6 + 0.029HIC$

PDFF: proton density fat fraction, $v_{(C, E, B, I)}$: volume fractions of the intracellular pool, extracellular fluid, blood, and interstitial fluid, f: off-resonance frequency. Both fat fraction and volume fractions are unitless. $R_{2(E, C)}$: transverse relaxation rates of extracellular fluid and intracellular pool, $R_{1(E, C)}$: longitudinal relaxation rates of extracellular fluid and intracellular pool.

* For the full characterization of fat, see data in Table 3.

Table 3 Fat peak parameters used in the Bloch simulation of the shMOLLI sequence. T_1 and T_2 values of fat peaks in peanut oil were measured at room temperature (20°C) for the phantom work and at human body temperature (37°C) for human experiments.

			Peanut oil (T = 20°C)		Participants (T = 37°C)	
Peak number	Chemical shift (relative to tetramethylsilane) [ppm]	Relative amplitude [a.u.]	T_1 ± SD [ms]	T_2 ± SD [ms]	T_1 ± SD [ms]	T_2 ± SD [ms]
1	0.90	0.087	264 ± 20	54 ± 3	333 ± 12†	83*
2	1.30	0.693	291 ± 21	61 ± 1	312 ± 17**	62*
3	2.10	0.128	231 ± 18	52 ± 3	254 ± 8†	52*
4	2.76	0.004	248 ± 25	61 ± 5	273 ± 8†	51*
5	4.30	0.039	193 ± 14	43 ± 2	228 ± 8†	49 ± 3†
6	5.30	0.049	285 ± 15	48 ± 2	332 ± 15†	50 ± 4†

*As reported by Hamilton et al.[39]

**As measured in livers of participants

†As measured in peanut oil

Table 4 Baseline parameter values for fat-water phantoms, as measured with multiple-contrast spin echo, shMOLLI, and multiple-TR STEAM ^{1}H MRS. Water T_2 and shMOLLI T_1 were averaged over circular regions of interest on corresponding maps.

$NiCl_2$ concentration [mM]	PDFF [%]	STEAM T_1 of water ± SD [ms]	T_2 of water ± SD [ms]	shMOLLI T_1 ± SD [ms]
0.45	0.0	1390 ± 30	78 ± 3	1294 ± 31
	7.0	1386 ± 24	*	1340 ± 29
	10.3	1425 ± 35	*	1433 ± 38
	15.6	1392 ± 29	*	1527 ± 42
	26.8	1386 ± 17	*	1736 ± 62
0.73	0.0	1148 ± 29	82 ± 2	1071 ± 18
	7.3	1177 ± 34	*	1132 ± 25
	11.1	1169 ± 20	*	1156 ± 21
	16.0	1136 ± 30	*	1236 ± 31
	24.7	1135 ± 28	*	1303 ± 39
1.61	0.0	690 ± 23	89 ± 5	627 ± 7
	6.8	690 ± 29	*	651 ± 7
	12.6	689 ± 27	*	680 ± 8
	21.5	684 ± 20	*	735 ± 11
	27.0	687 ± 16	*	798 ± 12

*As the MCSE experiment could not be used to determine water T_2 when mixed with fat, we have used the same water T_2 within a $NiCl_2$ concentration group as the T_2 measured in the 0% fat phantom of each group.

Table 5 Linear regression correlation coefficients for shMOLLI T_1 dependence on water STEAM T_1, PDFF and liver R_2^*, determined from original measured shMOLLI T_1 values, iron-corrected shMOLLI T_1 values, and iron-, fat-, and off-resonance-independent water shMOLLI T_1 values. Coefficients are shown as estimate ± standard error.

	STEAM T_1 coefficient [ms shMOLLI T_1/ms STEAM T_1]	P-value	PDFF coefficient [ms shMOLLI T_1/% PDFF]	P-value	R_2^* coefficient [ms shMOLLI T_1/s^{-1} R_2^*]	P-value
Measured shMOLLI T_1	0.5 ± 0.2	0.0051	11.7 ± 2.5	< 0.0010	-1.7 ± 0.4	< 0.0010
Iron-corrected shMOLLI T_1	0.8 ± 0.1	<0.0010	13.9 ± 2.1	< 0.0010	-0.4 ± 0.4	0.3544
Iron-, fat- and off-resonance-independent water shMOLLI T_1	0.7 ± 0.1	<0.0010	2.9 ± 1.7	0.1040	-0.6 ± 0.3	0.0400

SUPPLEMENTARY MATERIAL

Mapping tissue water T_1 in the liver using the MOLLI T1 method in the presence of fat, iron and B_0 inhomogeneity

METHODS

Table S1 summarizes the simulation parameters used for a water shMOLLI T_1 determination method that includes exchange effects between liver compartments.

Table S1 Simulation parameters for the liver model at 3 T. PDFF: proton density fat fraction, $v_{(S, L, E, B, I)}$: volume fractions of the intracellular semisolid pool, intracellular liquid pool, extracellular fluid, blood, and interstitial fluid, f: off-resonance frequency. Both fat fraction and volume fractions are unitless. $R_{2(B, I, E, S, L)}$: transverse relaxation rates of blood, interstitial fluid, extracellular fluid, semisolid intracellular pool and liquid intracellular pool, $R_{1(B, I, E, S, L)}$: longitudinal relaxation rates of blood, interstitial fluid, extracellular fluid, semisolid intracellular pool and liquid intracellular pool.

Parameter	Value
PDFF	Proton density fat fraction as measured by ^{1}H STEAM MRS
v_S	$0.07(1 - v_E - PDFF)$
v_L	$0.93(1 - v_E - PDFF)$
v_E	Simulated from 0.25 to $(0.95 - PDFF)$
v_B	$\frac{1 - v_E - PDFF}{3}$
v_I	$v_E - v_B$
f [Hz]	As determined from the multiple-echo GRE sequence
Fat chemical shifts [ppm]	As determined by the multiple-TR, multiple-TE STEAM ^{1}H MRS sequence of peanut oil
T_{1fat} [s]	T_1 of methylene peak determined from human ^{1}H spectra. Others as determined by the multiple-TR, multiple-TE STEAM ^{1}H MRS sequence of peanut oil.
T_{2fat} [s]	Values have been taken from the literature (1). Values for some of the peaks not available in the literature were determined from peanut oil spectra.
R_{2B} $[s^{-1}]$	$3.64 + (0.7 \times 26.06HIC^{0.701} - 0.7 \times 0.438HIC^{1.402}) \times 1.47$
R_{2I} $[s^{-1}]$	$2.9 + (0.7 \times 26.06HIC^{0.701} - 0.7 \times 0.438HIC^{1.402}) \times 1.47$
R_{2E} $[s^{-1}]$	$\frac{3.64v_B + 2.9v_I}{v_E} + 26.82HIC^{0.701} - 0.451HIC^{1.402}$
R_{2S} $[s^{-1}]$	$\frac{1}{7.7 \times 10^{-6}}$
R_{2L} $[s^{-1}]$	$11.0 + 46.0HIC^{0.701} - 0.773HIC^{1.402}$
R_{1B} $[s^{-1}]$	$0.518 + 0.029HIC$
R_{1I} $[s^{-1}]$	$0.44 + 0.029HIC$
R_{1E} $[s^{-1}]$	$\frac{0.518v_B + 0.44v_I}{v_E} + 0.029HIC$
R_{1S} $[s^{-1}]$	1.00
R_{1L} $[s^{-1}]$	$1.6 + 0.029HIC$
k_{LS} $[s^{-1}]$	$3.52/v_L$
k_{SL} $[s^{-1}]$	$3.52/v_S$
k_{LE} $[s^{-1}]$	$0.52/v_L$

k_{EL} [s^{-1}]	$0.52/v_E$

The water shMOLLI T_1 determination algorithm was built in a similar fashion to that presented in the main Methods section for patients, with the difference that instead of Bloch equations, Bloch-McConnell equations were simulated to model exchange between the semisolid and liquid pools of the intracellular compartment of the liver and the liquid pool of the intracellular compartment and the extracellular compartment.

The shMOLLI RF pulse sequence was simulated for each extracellular fluid volume fraction. Once separate signals for the semisolid intracellular pool, the liquid intracellular pool the extracellular pool and hepatic fat were simulated, they were combined to form the final bSSFP signal that was fitted using the shMOLLI conditional fitting algorithm (2).

RESULTS

Figure S1 presents the water shMOLLI T_1s determined when considering the iron- and fat concentrations and B_0 inhomogeneity alongside the results from iron-correction only. Figure S2 shows a significant ($P < 0.001$) drop in the variance of shMOLLI T_1 values when modelling the fat and B_0 inhomogeneities in addition to the iron on a Bland-Altman plot.

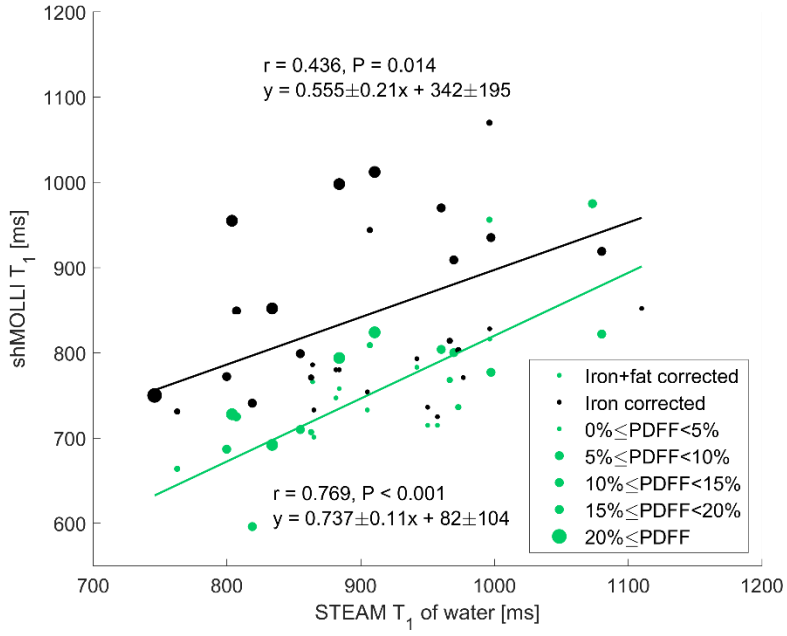

Figure S1 Correcting for fat increased the correlation between STEAM T_1 of the water in the liver and shMOLLI T_1 values. PDFF of individual data points is encoded in point size.

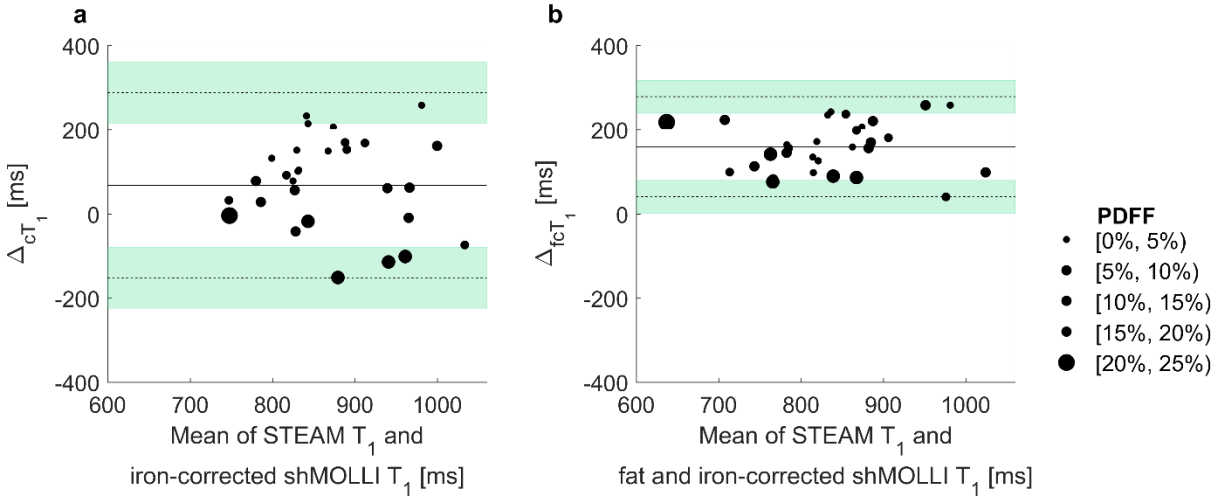

Figure S2 Bland-Altman plots showing patient data after iron-only (a) and after (b) iron-, fat- and off-resonance correction. The underestimation of T_1 values by the shMOLLI method explains the bias on the agreement plots. An F-test performed on the two differences shown in the subfigures revealed that the variance of measurements significantly decreased after the correction. Δ_{cT_1} is the difference between STEAM T_1 of the water in the liver and the iron-corrected shMOLLI T_1; Δ_{fcT_1} is the difference between STEAM T_1 of the water in the liver and the iron-, fat- and off-resonance-corrected shMOLLI T_1

Table S2 Linear regression correlation coefficients for water STEAM T_1, PDFF and liver R_2*, determined from original measured shMOLLI T_1 values, iron-corrected shMOLLI T_1s with MT and iron-corrected water shMOLLI T_1 values with MT and fat and B_0 inhomogeneity modelling. Coefficients are shown as estimate ± standard error.

	STEAM T_1 coefficient [ms shMOLLI T_1/ms STEAM T_1]	P-value	PDFF coefficient [ms shMOLLI T_1/% PDFF]	P-value	R_2^* coefficient [ms shMOLLI T_1/s^{-1} R_2^*]	P-value
Measured shMOLLI T_1	0.9 ± 0.1	<0.0001	13.2 ± 2.6	<0.0001	-1.6 ± 0.3	<0.0001
Iron-corrected shMOLLI T_1 with MT	0.9 ± 0.1	<0.0001	14.8 ± 2.3	<0.0001	-0.04 ± 0.4	0.9249
Iron-corrected water shMOLLI T_1 with MT and fat and B_0 inhomogeneity modelling	0.8 ± 0.1	<0.0001	2.5 ± 1.9	0.2028	-0.3 ± 0.3	0.4323

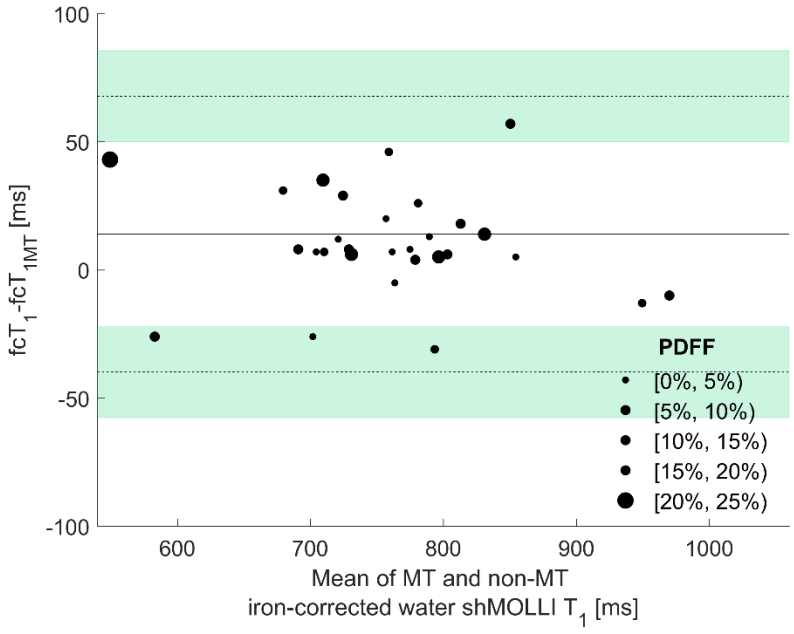

Figure S3 Bland-Altman plot showing that the MT-enabled correction is generally underestimating the non-MT-enabled correction. fcT_1 is a non-MT-enabled iron-corrected water shMOLLI T_1 with fat and B_0 inhomogeneity modelling and $fcT_{1_{MT}}$ is an MT-enabled iron-corrected water shMOLLI T_1 with fat and B_0 inhomogeneity modelling

A paired t-test between water shMOLLI T_1s with and without MT simulation has not revealed a significant difference between the two resulting sets of water shMOLLI T_1 values ($P = 0.528$). The values determined with MT simulation were numerically, but not significantly (left-tailed t-test $P = 0.4589$) lower than their non-MT-simulated counterparts, which has previously been shown to be the case (3) already.

Table S2 shows that all significant dependence on iron and fat is removed by our algorithm. The near-identical Pearson's correlation coefficients of the MT- and non-MT-enabled algorithms and the Bland-Altman plot shown in Figure S3 suggest that for all practical purposes the two algorithms produce very similar results.

Supporting References

1. Hamilton G, Schlein AN, Middleton MS, Hooker CA, Wolfson T, Gamst AC, et al. In vivo triglyceride composition of abdominal adipose tissue measured by ^{1}H MRS at 3T. J Magn Reson Imaging [Internet]. 2016 Aug [cited 2016 Sep 1]; Available from: http://doi.wiley.com/10.1002/jmri.25453

2. Piechnik SK, Ferreira VM, Dall'Armellina E, Cochlin LE, Greiser A, Neubauer S, et al. Shortened Modified Look-Locker Inversion recovery (ShMOLLI) for clinical myocardial T1-mapping at 1.5 and 3 T within a 9 heartbeat breathhold. J Cardiovasc Magn Reson [Internet]. 2010 Jan [cited 2015 Jan 12];12(1):69. Available from: http://www.jcmr-online.com/content/12/1/69

3. Tunnicliffe EM, Banerjee R, Pavlides M, Neubauer S, Robson MD. A model for hepatic fibrosis: the competing effects of cell loss and iron on shortened modified Look-Locker inversion recovery T_1 (shMOLLI-T_1) in the liver. J Magn Reson Imaging [Internet]. 2016 Jul [cited 2016 Sep 16]; Available from: http://doi.wiley.com/10.1002/jmri.25392